


Article

Effect of the Number of Anchoring and Electron-Donating Groups on the Efficiency of Free-Base- and Zn-Porphyrin-Sensitized Solar Cells

Raheleh Nasrollahi ^{1,2}, Luis Martín-Gomis ¹, Fernando Fernández-Lázaro ¹, Saeed Zakavi ²  and Ángela Sastre-Santos ^{1,*} 

¹ Área de Química Orgánica, Instituto de Bioingeniería, Universidad Miguel Hernández, Avda. de la Universidad s/n, 03203 Elche, Spain; rnasrolahi@iasbs.ac.ir (R.N.); luis.martin@umh.es (L.M.-G.); fdofdez@umh.es (F.F.-L.)

² Department of Chemistry, Institute for Advanced Studies in Basic Sciences (IASBS), Zanjan 45137-66731, Iran; zakavi@iasbs.ac.ir

* Correspondence: asastre@umh.es; Tel.: +34-96-6658-408

Received: 29 December 2018; Accepted: 15 February 2019; Published: 21 February 2019



Abstract: A series of porphyrin compounds, free base (H₂P) and their Zn (II) metallated analogues (ZnP), bearing one, two or three carboxylic acid groups, have been synthesized, characterized, and used as sensitizers in dye sensitized solar cells (DSSCs). The performance of these devices has been analyzed, showing higher efficiencies of those sensitized with ZnP compounds. These results have been explained, on one hand, taking into account the electronic character of the metal ion, which acts as mediator in the injection step, and, on the other, considering the number of anchoring groups, which determines both the stereoelectronic character of the dye and the way it binds to TiO₂ surface.

Keywords: porphyrins; DSSC; multiple anchoring group; electron donating groups

1. Introduction

Porphyrins [1] have been extensively used as key components in different organic optoelectronic applications. Thanks to their aromatic nature, porphyrins present interesting light absorption/emission and electroactive properties, easily tunable due to their chemical versatility [2,3]. With these elements, it is possible to find in the literature a myriad of different porphyrin compounds, chemically designed to fulfill technological requirements in a variety of fields [4,5]. Dye sensitized solar cells (DSSC) [6–8] is one of these fields where porphyrin compounds have been widely employed, usually playing the role of sensitizing dyes. After thorough investigations, there is a general agreement on the structural requirements of porphyrins to be used in DSSCs: 1) at least one anchoring group must be present for the covalent binding to the semiconductor surface [9], 2) metallic complexes (MP), especially the zinc ones, are preferred to free-base (H₂P), because of their longer-lived singlet excited states and much lower oxidation potentials [10], and 3) bulky electron-donor meso-substituents favor electron injection in the semiconductor, as they originate an intrinsic dipole moment [11]. High efficiencies have been achieved for TiO₂-based devices sensitized, for example, with free-base [12] and zinc porphyrin derivatives [13], presenting one or more carboxylic acid appends as anchoring groups, either in β [9,14] or meso [15,16] positions of the porphyrin central core, and also with multiple donor groups at the meso positions [17–19]. The combination of the donor groups, and the electron-withdrawing carboxy group, contributes to create the push–pull effect, channelling the photoexcited electrons toward TiO₂ and improving charge separation.

Till now few examples analyzing the photovoltaic performance of DSSC devices sensitized with porphyrin dyes as a function of the number of anchoring groups have been reported [20–23]. Here we present the synthesis and characterization of a series of free-base porphyrins with one, two, and three carboxy groups, H_2P-CO_2H **1**, $cis-H_2P-(CO_2H)_2$ **2-c**, $H_2P-(CO_2H)_3$ **3**, and their Zn metalated analogues $ZnP-CO_2H$ **4**, $cis-ZnP-(CO_2H)_2$ **5-c** and $ZnP-(CO_2H)_3$ **6** (Figure 1). Also, the number of electron donating $-OCH_3$ groups, decreased in the series from nine (in **1** and **4**) to three (in **3** and **6**), and this is expected to tune the energy of the porphyrin frontier orbitals, influencing the π resonance interactions between porphyrin and aryl group π systems. All of them were then incorporated in efficient dye sensitized solar devices, comparing the performance obtained in terms of the number of anchoring carboxy and electron-donating $-OCH_3$ groups, and the presence of zinc as metallic central ion.

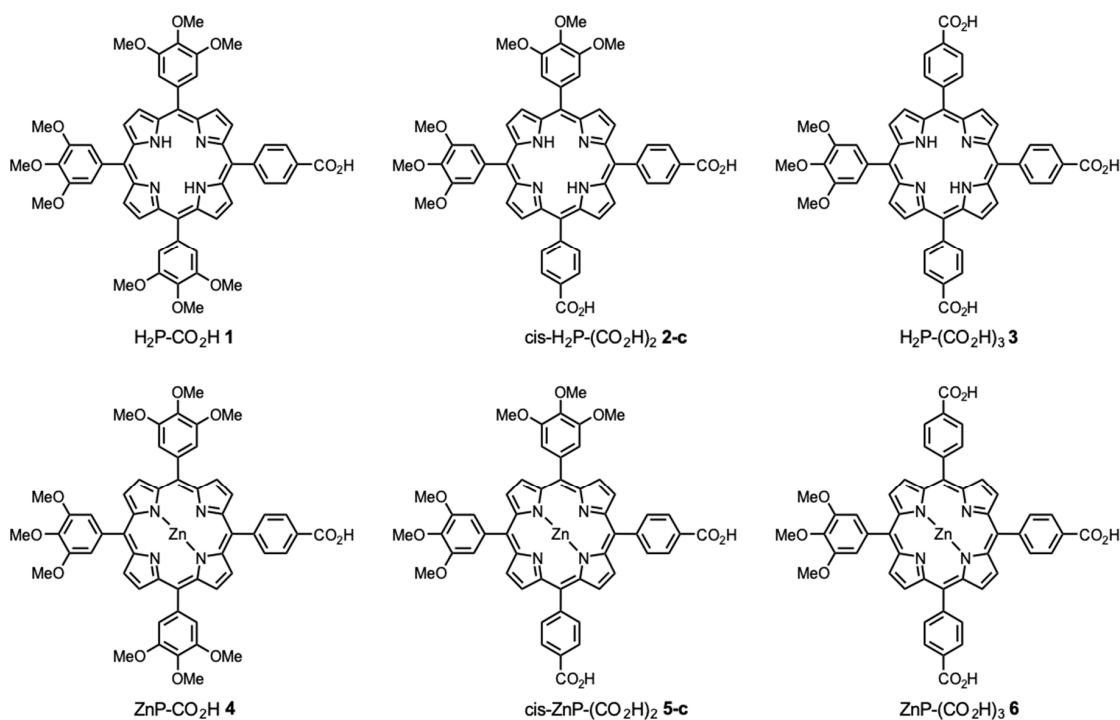


Figure 1. Molecular structures of porphyrin-based sensitizers used in this study.

2. Materials and Methods

2.1. Synthesis and Characterization of New Compounds

All chemicals were reagent grade, purchased from commercial sources, and were used as received unless otherwise specified. Column chromatography was performed on SiO_2 (40–63 μm). TLC plates coated with SiO_2 60F254 were visualized under UV light. NMR spectra were acquired on a Bruker AC 300 spectrometer (Bruker, Billerica, MA, USA). UV/Vis spectra were recorded on a Helios Gamma spectrophotometer. Fluorescence spectra were recorded on a Perkin-Elmer LS 55 luminescence spectrometer (PerkinElmer, Waltham, MA, USA). Matrix-assisted laser desorption/ionization time-of-flight (MALDI-TOF) mass spectra were obtained on a Bruker Microflex spectrometer (Bruker, Billerica, MA, USA). Differential pulse voltammetry measurements were performed at 298 K in a conventional three-electrode cell using a m-AUTOLAB type III potentiostat/galvanostat (Metrohm, Herisau, Switzerland). Sample solutions (ca. 0.5 mM) were prepared in deaerated PhCN, containing 0.10 M tetrabutylammonium hexafluorophosphate (TBAPF₆) as supporting electrolyte. A glassy carbon (GC) working electrode, an Ag/AgNO₃ reference electrode, and a platinum wire counter electrode were used. Ferrocene/ferrocenium was the internal standard for all measurements.

2.1.1. Synthesis of Free-Base Porphyrins $H_2P-(CO_2Me)_n$ 7–9

In a 500 mL round bottom flask equipped with a magnetic stirrer, 3.53 g of 3,4,5-trimethoxy benzaldehyde (18 mmol), 0.99 g of methyl 4-formylbenzoate (6 mmol) and 1.65 mL of pyrrole (24 mmol) were refluxed for 5 h in propionic acid (250 mL). After cooling at room temperature, the resulting mixture was extracted with dichloromethane several times and, the combined extracts, washed with water and aqueous 4% $NaHCO_3$ solution, dried over $MgSO_4$ and evaporated. The black colored crude compound was purified by silica gel column using hexane/ethylacetate eluent mixtures to get 0.396 g (7%) of 7 H_2P-CO_2Me , 0.437 g (8%) of a mixture of 8 $H_2P-(CO_2H)_2$ cis and trans isomers and 0.422 g (8%) of 9 $H_2P(CO_2H)_3$.

5-(4-methoxycarbonylphenyl)-10,15,20-tris(3,4,5-trimethoxyphenyl)porphyrin (H_2P-CO_2Me 7). 1H NMR ($CDCl_3$: 300 MHz), δ ppm: -2.78 (s, 2H, $-NH$), 3.97 (s, 18H, $m-OCH_3$), 4.12 (s, 3H, $-OCH_3$) 4.19 (s, 9H, $p-OCH_3$), 7.47 (s, 6H, phenyl H), 8.32 (d, 2H, phenyl H), 8.44 (d, 2H, phenyl H), 8.81 (d, 2H, pyrrole H), 8.98 (d, 6H, pyrrole H). UV-vis (THF) λ_{max}/nm ($\log \epsilon$): 420 (5.64), 515 (4.36), 550 (3.98), 592 (3.74), 650 (3.00). HRMS (MALDI-TOF): m/z calcd, for $C_{55}H_{50}N_4O_{11}$ ($[M^+]$): 942.35, found 942.43.

5,10-bis(4-methoxycarbonylphenyl)-15,20-bis(3,4,5 trimethoxyphenyl)porphyrin ($H_2P-(CO_2Me)_2$ 8, cis/trans mixture). 1H NMR ($CDCl_3$: 300 MHz), δ ppm: -2.79 (s, 2H, $-NH$), 3.97 (s, 12H, $m-OCH_3$), 4.11 (s, 6H, $-OCH_3$) 4.18 (s, 6H, $p-OCH_3$), 7.46 (s, 4H, phenyl H), 8.31 (d, 4H, phenyl H), 8.44 (d, 4H, phenyl H), 8.81 (d, 4H, pyrrole H), 8.97 (d, 4H, pyrrole H). UV-vis (THF) λ_{max}/nm ($\log \epsilon$): 421 (5.58), 515 (4.29), 549 (3.88), 591 (3.68), 649 (3.18). HRMS (MALDI-TOF): m/z calcd, for $C_{54}H_{46}N_4O_{10}$ ($[M^+]$): 910.32, found 910.45.

5,10,15-tris(4-methoxycarbonylphenyl)-20-(3,4,5-trimethoxyphenyl)porphyrin ($H_2P-(CO_2Me)_3$ 9). 1H NMR ($CDCl_3$: 300 MHz), δ ppm: -2.80 (s, 2H, $-NH$), 3.97 (s, 6H, $m-OCH_3$), 4.12 (s, 9H, $-OCH_3$) 4.18 (s, 3H, $p-OCH_3$), 7.46 (s, 2H, phenyl H), 8.31 (d, 2H, phenyl H), 8.43 (d, 2H, phenyl H), 8.81 (d, 2H, pyrrole H), 8.98 (d, 2H, pyrrole H). UV-vis (THF) λ_{max}/nm ($\log \epsilon$): 419 (5.44), 514 (4.13), 550 (3.73), 590 (3.48), 649 (2.30). HRMS (MALDI-TOF): m/z calcd, for $C_{53}H_{42}N_4O_9$ ($[M^+]$): 878.30, found 878.64.

2.1.2. Synthesis of Free-Base Porphyrins $H_2P-(CO_2H)_n$ 1–3:

50 mg of free-base porphyrin was dissolved in a mixture of THF/MeOH (20/14 mL) and 6 mL of NaOH 20% aqueous solution were added. The crude was heated for 2 h. After cooling, the reaction crude was then diluted with dichloromethane and washed, first with HCl (1M) and then with water. The organic layer dried over $MgSO_4$ and evaporated. The residue was recrystallized in hexane to get the pure powder.

Column chromatography was conducted for $H_2P-(CO_2H)_2$ 2, to isolate cis and trans isomers (SiO_2 , chloroform/acetone mixtures as eluents).

5-(4-carboxyphenyl)-10,15,20-tris(3,4,5-trimethoxyphenyl)porphyrin (H_2P-CO_2H 1). Yield: 95%. 1H NMR (DMSO: 300 MHz), δ ppm: -2.93 (s, 2H, $-NH$), 3.90 (s, 18H, $m-OCH_3$), 4.00 (s, 9H, $p-OCH_3$), 7.53 (s, 2H, phenyl H), 8.33 (d, 2H, phenyl H), 8.39 (d, 2H, phenyl H), 8.81 (d, 2H, pyrrole H), 8.96 (d, 6H, pyrrole H). UV-vis (THF) λ_{max}/nm ($\log \epsilon$): 420(5.38), 515(4.13), 550(3.70), 592(3.70), 650 (3.30). HRMS (MALDI-TOF) calcd for $C_{54}H_{48}N_4O_{11}$ ($[M^+]$): 928.33, found 928.38.

5,10-bis(4-carboxyphenyl)-15,20-bis(3,4,5 trimethoxyphenyl)porphyrin, trans isomer (trans- $H_2P-(CO_2H)_2$ 2-t). Yield: 23%. 1H NMR (DMSO: 300 MHz), δ ppm: -2.93 (s, 2H, $-NH$), 3.89 (s, 12H, $m-OCH_3$), 3.99 (s, 6H, $p-OCH_3$), 7.54 (s, 4H, phenyl H), 8.33 (d, 4H, phenyl H), 8.38 (d, 4H, phenyl H), 8.82 (d, 4H, pyrrole H), 8.98 (d, 4H, pyrrole H). UV-vis (THF) λ_{max}/nm ($\log \epsilon$): 420 (5.59), 515 (4.27), 550 (3.93), 592 (3.78), 651(3.65). HRMS (MALDI-TOF): m/z calcd, for $C_{52}H_{42}N_4O_{10}$ ($[M^+]$): 882.29, found 882.518.

5,10-bis(4-carboxyphenyl)-15,20-bis(3,4,5-trimethoxyphenyl)porphyrin, cis isomer (cis-H₂P-(CO₂H)₂ 2-c). Yield: 71%. ¹H NMR (DMSO: 300 MHz), δ ppm: −2.93 (s, 2H, −NH), 3.90 (s, 12H, m−OCH₃), 3.99 (s, 6H, p−OCH₃), 7.53 (s, 4H, phenyl H), 8.32 (d, 4H, phenyl H), 8.38 (d, 4H, phenyl H), 8.83 (d, 4H, pyrrole H), 8.98 (d, 4H, pyrrole H). UV-vis (THF) λ_{max}/nm (log ε): 420 (5.59), 515 (4.27), 550 (3.93), 591 (3.78), 649 (3.65). HRMS (MALDI-TOF): m/z calcd, for C₅₂H₄₂N₄O₁₀ ([M⁺]): 882.29, found 882.52.

5,10,15-tris(4-carboxyphenyl)-20-(3,4,5-trimethoxyphenyl)porphyrin (H₂P-(CO₂H)₃ 3). Yield: 94%. ¹H NMR (DMSO: 300 MHz), δ ppm: −2.93 (s, 2H, −NH), 3.90 (s, 6H, m−OCH₃), 3.99 (s, 3H, p−OCH₃), 7.55 (s, 2H, phenyl H), 8.35 (d, 6H, phenyl H), 8.38 (d, 6H, phenyl H), 8.85 (d, 6H, pyrrole H), 8.98 (d, 2H, pyrrole H). UV-vis (THF) λ_{max}/nm (log ε): 419(5.52), 515(4.18), 549(3.78), 590(3.54), 649 (3.40). HRMS (MALDI-TOF): m/z calcd, for C₅₀H₃₆N₄O₉ ([M⁺]): 836.25, found 836.50.

2.1.3. Synthesis of Zinc Porphyrins ZnP-(CO₂H)_n 4–6

Free-base porphyrin (7, 8 or 9, 50 mg) and zinc acetate (1:5 mol ratio) were refluxed in dichloromethane and methanol (1:1 ratio, 40 mL each) until free-base porphyrin was completely metalated, checked by TLC and UV-vis absorption spectroscopy. The reaction mixture was then diluted with dichloromethane and washed, first with HCl (1 M) and then with water. The organic layer was collected and, after evaporation of solvent, the crude compound was purified by silica gel column using hexane/ethyl acetate eluent mixtures. Quantitative yields were obtained in all cases and isolated compounds were hydrolyzed following the same procedure used for free-base porphyrins hydrolysis (see Section 2.1.2).

Column chromatography was conducted for ZnP-(CO₂H)₂ 5 to isolate cis and trans isomers (SiO₂, chloroform/acetone mixtures as eluents).

Zinc(II) 5-(4-carboxyphenyl)-10,15,20-tris(3,4,5-trimethoxyphenyl)porphyrinate (ZnP-CO₂H 4). Yield: 98%. ¹H NMR (DMSO: 300 MHz), δ ppm: 3.90 (s, 18H, m−OCH₃), 3.99 (s, 9H, p−OCH₃), 7.45 (s, 2H, phenyl H), 8.29 (d, 2H, phenyl H), 8.37 (d, 2H, phenyl H), 8.75 (d, 2H, pyrrole H), 8.90 (d, 6H, pyrrole H). UV-vis (THF) λ_{max}/nm (log ε): 426 (5.63), 557 (4.20), 597 (3.65). HRMS (MALDI-TOF) calcd for C₅₄H₄₆N₄O₁₁ ([M⁺]): 990.25, found 989.22.

Zinc(II) 5,10-bis(4-carboxyphenyl)-15,20-bis(3,4,5-trimethoxyphenyl)porphyrinate, trans isomer (trans-ZnP-(CO₂H)₂ 5-t). Yield: 20%. ¹H NMR (DMSO: 300 MHz), δ ppm: 3.89 (s, 12H, m−OCH₃), 3.98 (s, 6H, p−OCH₃), 7.46 (s, 4H, phenyl H), 8.23 (d, 4H, phenyl H), 8.35 (d, 4H, phenyl H), 8.76 (d, 4H, pyrrole H), 8.91 (d, 4H, pyrrole H). HRMS (MALDI-TOF): m/z calcd, for C₅₂H₄₀N₄O₁₀Zn ([M⁺]): 944.20, found 943.45.

Zinc (II) 5,10-bis(4-methoxycarbonylphenyl)-15,20-bis(3,4,5-trimethoxyphenyl)porphyrinate, cis isomer (cis-ZnP-(CO₂H)₂ 5-c). Yield: 69%. ¹H NMR (DMSO: 300 MHz), δ ppm: 3.89 (s, 12H, m−OCH₃), 3.98 (s, 6H, p−OCH₃), 7.45 (s, 4H, phenyl H), 8.23 (d, 4H, phenyl H), 8.34 (d, 4H, phenyl H), 8.76 (d, 4H, pyrrole H), 8.91 (d, 4H, pyrrole H). UV-vis (THF) λ_{max}/nm (log ε): 426 (5.56), 557 (4.29), 597 (3.80). HRMS (MALDI-TOF): m/z calcd, for C₅₂H₄₀N₄O₁₀Zn ([M⁺]): 944.20, found 943.48.

Zinc(II) 5,10,15-tris(4-carboxyphenyl)-20-(3,4,5-trimethoxyphenyl)porphyrinate (ZnP-(CO₂H)₃ 6). Yield: 98%. ¹H NMR (DMSO: 300 MHz), δ ppm: 3.90 (s, 6H, m−OCH₃), 3.99 (s, 3H, p−OCH₃), 7.47 (s, 2H, phenyl H), 8.29 (d, 6H, phenyl H), 8.37 (d, 6H, phenyl H), 8.78 (d, 6H, pyrrole H), 8.94 (d, 2H, pyrrole H). UV-vis (THF) λ_{max}/nm (log ε): 426 (5.70), 557 (4.33), 598 (3.89). HRMS (MALDI-TOF): m/z calcd, for C₅₀H₃₄N₄O₉Zn ([M⁺]): 898.16, found 897.40.

2.2. Device Preparation

Double-layered nanoporous TiO₂ photoanodes were prepared coating pastes of anatase TiO₂ nanoparticles having two different diameters, 20 nm (Dyesol's 90 T) and 400 nm (Dyesol's WER2-O), onto TiCl₄ treated FTO glass plates (TEC 15 A, 2.2 mm, Xop Glass), by repetitive screen printing to obtain

the required thickness. These electrodes were gradually heated under a programmed flow: at 370 °C for 10 min and 450 °C for 10 min. Their apparent surface area was 0.16 cm² (0.4 cm × 0.4 cm), and revealed a total thickness of 8–10 μm, containing a 3–4 μm scattering layer. The TiO₂ electrodes were treated again with TiCl₄ under 70 °C for 30 min and sintered at 500 °C for 30 min, before they were dipped into dye solution. The nanocrystalline TiO₂ films were immersed into 5 mM dye solutions, without any other additives, i.e. co-adsorbents, and kept at RT for 20 h. Finally, dye adsorbed TiO₂ photoanodes and thermally platinized and drilled FTO counter electrodes (TEC 8 A, 3 mm, Xop Glass), were assembled into sandwich type cells, separated by a 30 μm thick hot-melt gasket (Surllyn, Dupont), and sealed by heating. An electrolyte solution (0.1 M LiI, 0.03 M I₂, 0.5 M 4-*tert*-butylpyridine, 0.1 M guanidinium thiocyanate, 1 M 1-butyl-3-methylimidazolium iodide in acetonitrile/valeronitrile 85:15 v/v) was introduced in the assembled devices. A series of three devices with each dye were prepared and their photovoltaic performance measured. The values described are, in all cases, the best obtained, with no significant differences between devices sensitized with the same dye, which ensures the reproducibility and consistency of the results.

2.3. Photovoltaic Characterization

An ABET 150W xenon light source equipped with an AM 1.5 G correcting filter was employed. The light intensity was adjusted to 100 mW/cm² (the equivalent of 1 sun), prior to every measurement, using a calibrated photovoltaic reference cell (15150, ABET Technologies). The applied potential and cell current were registered with a Keithley 2401 low voltage digital sourcemeter. The incident photon-to-current conversion efficiency (IPCE) was measured as a function of wavelength from 400 to 800 nm by using an IPCE-DC system (Lasing SA).

3. Results and Discussion

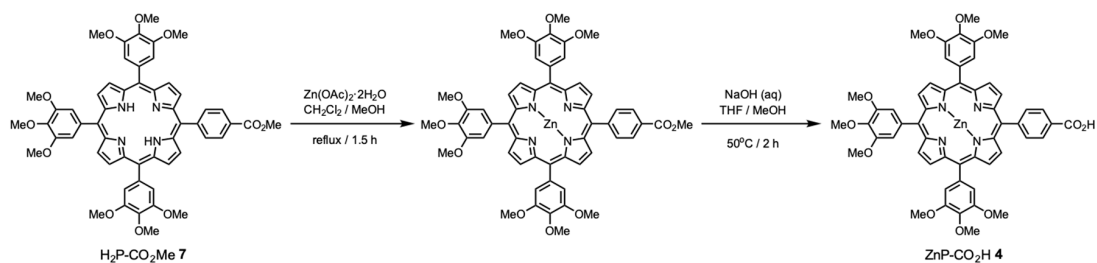
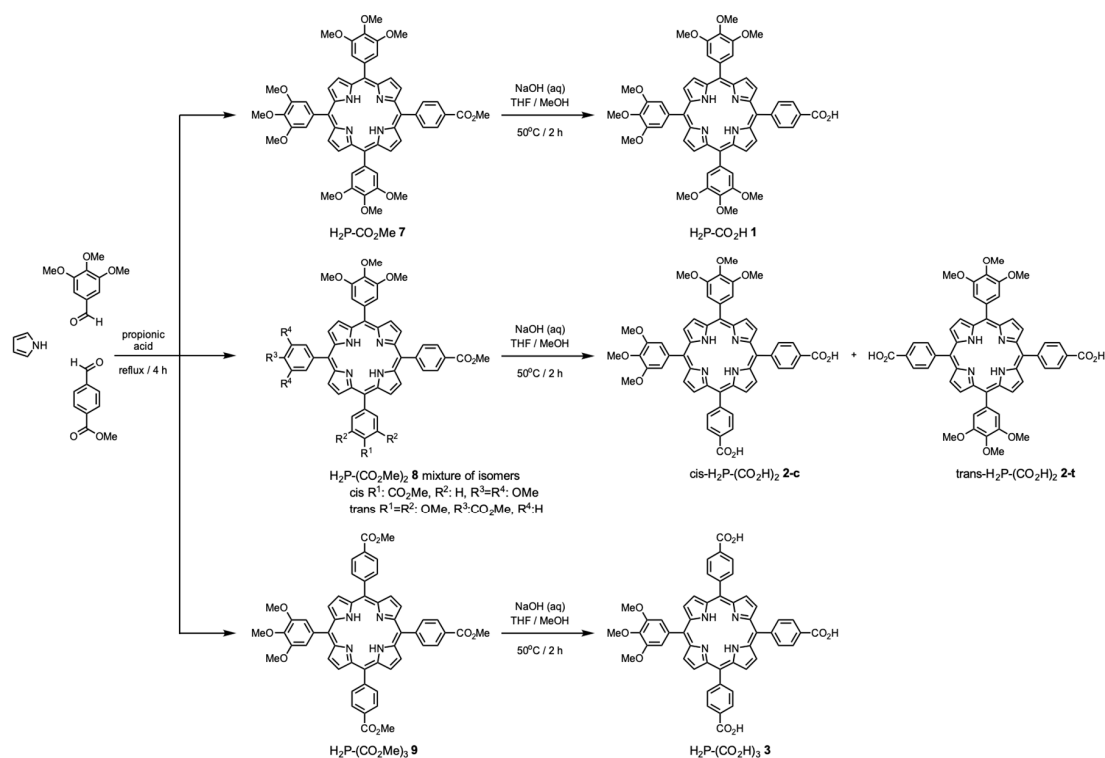
3.1. Synthesis of New Compounds

Free base porphyrin compounds H₂P-CO₂H **1**, H₂P-(CO₂H)₂ **2** (cis and trans) and H₂P-(CO₂H)₃ **3** were prepared through a two-step synthetic sequence, as it is described in Scheme 1. First, methyl ester derivatives (7–9) were obtained as pure compounds, following the traditional Adler-Longo method [24], by reacting a 4:3:1 mixture of pyrrole, 3,4,5-trimethoxybenzaldehyde and methyl 4-formylbenzoate in propionic acid. In a second step, methyl ester groups were hydrolyzed by heating in an aqueous base solution affording, in almost quantitative yields, free-base porphyrins with one, two and three carboxylic groups (1–3). It is worth to note that the hydrolysis of H₂P-(CO₂Me)₂ **8**, mixture of cis and trans stereoisomers, gave a new mixture which could be resolved into its components, cis-H₂P-(CO₂H)₂ **2-c** and trans-H₂P-(CO₂H)₂ **2-t**, through standard column chromatography.

Finally, in order to obtain Zn porphyrins ZnP-CO₂H **4**, ZnP-(CO₂H)₂ **5** (cis and trans) and ZnP-(CO₂H)₃ **6**, methyl ester precursors (7–9) were, first metallated in refluxing dichloromethane/methanol mixture, in presence of a zinc acetate excess, and, without isolation, hydrolyzed, following the procedure previously used in the synthesis of H₂P-(CO₂H)_n 1–3. An example of the synthetic sequence performed (synthesis of ZnP-CO₂H **4**) is shown in Scheme 2. As it occurred with H₂P-(CO₂H)₂ **2** cis and trans isomers, the metalation of **8** (mixture of isomers), followed by basic hydrolysis, afforded a new mixture of compounds which could be separated into its components, ZnP-(CO₂H)₂ **5** cis and trans, through standard column chromatography.

All synthesized compounds 1–9 (Figures S1, S4, S10, S13, S16, S19, S22, S25, S28 and S31) were characterized through common techniques, such ¹H NMR and UV-vis spectroscopies and HR-MS (MALDI TOF) mass spectrometry. In this context, the ¹H NMR signals obtained for H₂P-(CO₂H)_n 1–3 (Figures S2, S5, S7, S8 and S11), ZnP-(CO₂H)_n 4–6 (Figures S14, S17, S20, and S23) and H₂P-(CO₂Me)_n 7–9 (Figures S26, S29, and S32) showed similar chemical displacements, but displayed different integral values for the signals corresponding to the phenyl and methoxy groups. On the other hand, HR MS

gave, in all cases, a single peak with a m/z ratio that exactly matched the calculated one (Figures S3, S6, S9, S12, S15; S18, S21, S24, S27, S30 and S33).



3.2. Optical and Electrochemical Properties

Free porphyrins **1**, **2** cis, and **3**, and zinc derivatives, **4**, **5** cis, and **6**, were evaluated as sensitizers for DSSC devices. It must be stated that trans isomers of compounds **2** and **5** could not be evaluated, because of their reduced solubility which prevented their optical and electrochemical characterisation.

The UV-vis absorption spectra of all dyes show typical features of porphyrin compounds (Figure 2). While H_2P **1–3** present a strong absorption band at 420 nm ($S_0 \rightarrow S_2$, Soret band) and four weak transitions to the first excited state between 500 and 680 nm ($S_0 \rightarrow S_1$, Q bands), ZnP **4–6** exhibit, a 6–7 nm red-shifted Soret band and only two Q bands, which are located in the 550–650 nm area. These spectral changes, upon metalation of the macrocycle, are probably due to the increased symmetry of the porphyrin core, moving from D_{2h} to D_{4h} . It is also worth to note that the introduction of a zinc atom in the porphyrin cavity, causes a π - π interaction between the metal p_π orbital and the porphyrin π system. According to the four orbital model of porphyrins [25], the electronic density on the meso positions and the pyrrolic nitrogen atoms is large, so the energy of a_{2u} and e_g orbitals is, therefore, influenced by both the metal ion and the substituents introduced at the meso positions. Regarding to the molar extinction coefficients, zinc derivatives show somehow higher values than

the metal free ones. It is also remarkable that within a series (ZnP/H₂P), variations in the coefficients are minimal, and are attributed to differences in solubility, due to number of carboxy groups. Finally, internal conversion between S₂ and S₁ is rapid, so fluorescence is only detected from S₁. Taking into account that intensity of Q bands is weak, transition energies cannot be accurately estimated from the intersection of normalized absorption and emission spectra [26,27], so the optical band gap (E_g^{opt}) was here calculated using the equation (1) where λ_{edge} is the onset value of the absorption spectrum in the direction of longer wavelengths [28].

$$E_g^{\text{opt}} = \frac{1240}{\lambda_{\text{edge}}} \text{eV} \quad (1)$$

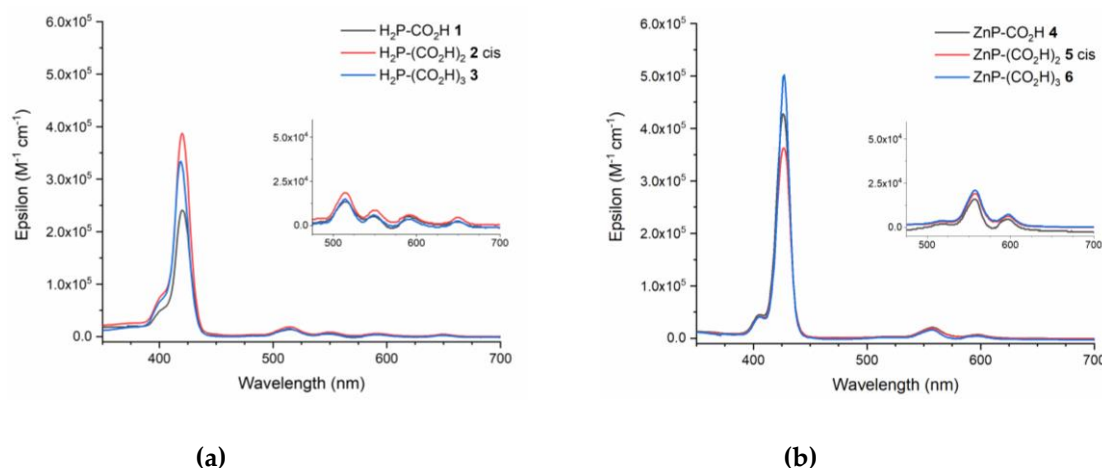


Figure 2. UV-Vis absorption spectra (350–700 nm) for (a) 1–3 and (b) 4–6 dyes, in THF solution.

Peak position (λ_{abs}), molar absorption coefficients (ε) of Soret and Q bands, onset values (λ_{edge}) and estimated optical band gap (E_g^{opt}) of porphyrin dyes are listed in Table 1.

Table 1. Absorption wavelengths, molar absorption coefficients, onset values and estimated optical band gaps of dyes 1–6.

Dye	λ _{abs} /nm (log ε)	λ _{edge} (nm)	E _g ^{opt} (eV)
H ₂ P-CO ₂ H 1	420 (5.38), 515 (4.13), 550 (3.70), 592 (3.70), 650 (3.30)	665.2	1.86
cis-H ₂ P-(CO ₂ H) ₂ 2-c	420 (5.59), 515 (4.27), 550 (3.93), 591 (3.78), 649 (3.65)	665.2	1.86
H ₂ P-(CO ₂ H) ₃ 3	419 (5.52), 515 (4.18), 549 (3.78), 590 (3.54), 649 (3.40)	665.2	1.86
ZnP-CO ₂ H 4	426 (5.63), 557 (4.20), 597 (3.65)	615.0	2.02
cis-ZnP-(CO ₂ H) ₂ 5-c	426 (5.56), 557 (4.29), 597 (3.80)	615.0	2.02
ZnP-(CO ₂ H) ₃ 6	426 (5.70), 557 (4.33), 598 (3.89)	615.0	2.02

Electrochemical measurements were performed for H₂P 1–3 and ZnP 4–6, registering differential pulse voltammograms in benzonitrile solution (Figure 3). All measured dyes exhibit simple, clear and sharp waves in the anodic part, very different from those in the cathodic area. This can be probably due to the genuine electron-donor character of porphyrin compounds and, particularly, for these studied 3,4,5-trimethoxyphenyl-substituted porphyrins. Also, this observation provides evidence for extensive changes in the electronic structure of the studied compounds, induced by one electron reduction of the aromatic macrocycles. In this context, and taking into account only oxidation processes, H₂P 1–3 are more resistant to oxidation than ZnP 4–6. On the other hand, as a general tendency, oxidation potentials increase with the number of carboxy groups. Due to the increase in the number of carboxy groups, which is associated with a concomitant decrease in the number of trimethoxyphenyl moieties, the resonance interactions between the a_{2u} orbital and the porphyrin π system become weaker, thus favoring the stabilization of that orbital. The decreased oxidation

potential of the metalloporphyrins, compared to that of the free base analogues, seems to be due to destabilization of a_{2u} orbitals of the former, probably caused by π resonance interactions between the metal p_{π} orbital, porphyrin a_{2u} orbital and the aryl group π system [29].

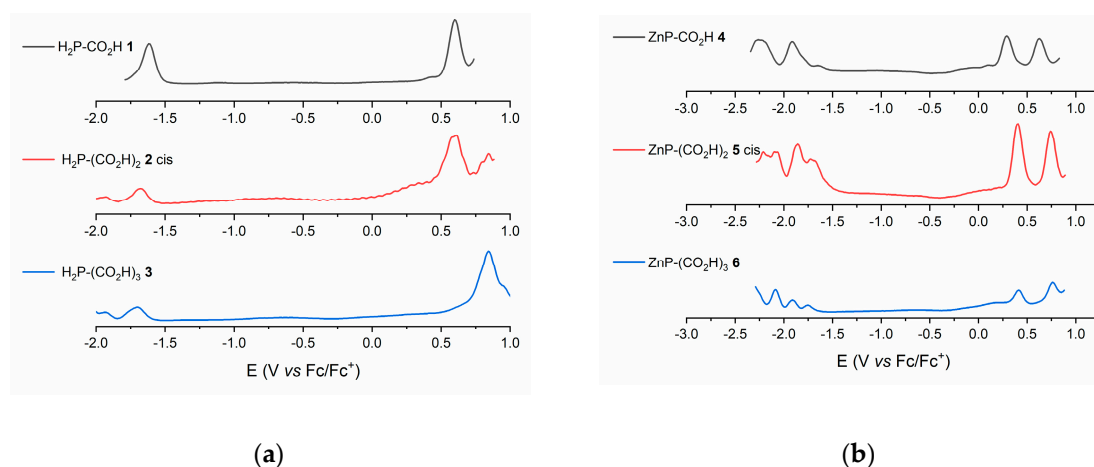


Figure 3. Differential pulse voltammograms of (a) 1–3 and (b) 4–6 dyes, registered in benzonitrile solution and using, tetra-butyl ammonium hexafluorophosphate (Bu_4NPF_6) as supporting electrolyte, platinum wire, glassy carbon and non-aqueous Ag/AgNO_3 as counter, working and reference electrodes, respectively, and ferrocene (Fc/Fc^+) as internal standard.

Spectral and electrochemical properties allow to determine the electron injection and dye regeneration possibility during DSSC performance. From E_{ox} potential values, referenced to Fc/Fc^+ pair, (Table 2) HOMO energy level for all dyes can be easily calculated, using the Equation (2).

$$E_{\text{HOMO}}(\text{eV}) = -4.8 - E_{\text{ox}}(\text{V vs Fc}/\text{Fc}^+) \quad (2)$$

Table 2. Oxidation potentials of dyes 1–6.

Dye	$\text{H}_2\text{P}-\text{CO}_2\text{H}$ 1	cis- $\text{H}_2\text{P}-(\text{CO}_2\text{H})_2$ 2-c	$\text{H}_2\text{P}-(\text{CO}_2\text{H})_3$ 3	$\text{ZnP}-\text{CO}_2\text{H}$ 4	cis- $\text{ZnP}-(\text{CO}_2\text{H})_2$ 5-c	$\text{ZnP}-(\text{CO}_2\text{H})_3$ 6
E_{ox} (V)	0.60	0.60	0.84	0.29	0.39	0.42

These values, combined with the previously estimated optical band gap (E_g^{opt}), and values of conduction band of TiO_2 (-4.2 eV) [30] and I^-/I_3^- redox potential (-4.89 eV) [31,32], allow to sketch an energy diagram representing HOMO and LUMO levels for all studied dyes (Figure 4). At this point, it is important to mention that the determination of the LUMO level, using the E_{HOMO} obtained from electrochemical measurements and estimated E_g^{opt} , is a very useful approximation in the case that both E_{ox} and E_{red} values cannot be accurately extracted from electrochemical measurements. As can be seen, LUMO energy levels are, in all cases, higher than TiO_2 conduction band (TiO_2 CB), fundamental requisite to make the electron injection thermodynamically feasible, while HOMO levels are, always, lower than I^-/I_3^- redox potential, making possible the regeneration of the oxidized dye.

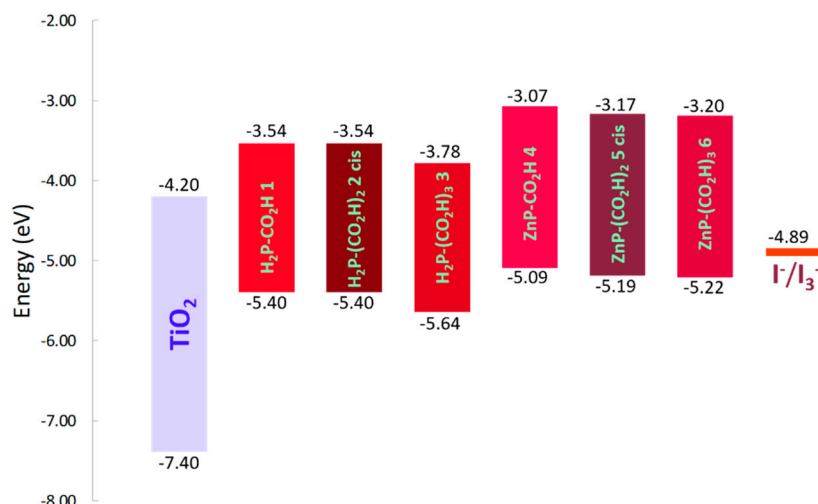


Figure 4. Energy level diagram sketched from spectral and electrochemical data.

3.3. Preparation of Devices and Photovoltaic Characterization

Dye sensitized solar cells were prepared following a standard procedure, using double layered screen-printed TiO₂ photoanodes, platinum casted counter-electrodes, and liquid electrolyte containing 0.05 M LiI, 0.03 M I₂, 0.5 M 4-*tert*butylpyridine (TBP), 0.1 M guanidinium thiocyanate (GNCS), 1 M 1-butyl-3-methylimidazolium iodide (BMII) in acetonitrile/valeronitrile (85:15 v/v). Once prepared, efficiencies of all devices were evaluated under standard Air Mass 1.5 global (AM1.5G) solar irradiation, constructing J/V curves, and analyzing incident photon to current conversion efficiencies (IPCE).

All employed dyes gave efficient photoanode sensitization without any other additive (20 h dipping in 5 mM dye ethanol solution), qualitatively appreciated through a deep anode coloration. At this point we considered the use of co-adsorbents to improve the performance, particularly chenodeoxycolic acid (Cheno). In porphyrin and phthalocyanine sensitized solar cells, Cheno is commonly used as co-adsorbent and, directly incorporated in sensitizing solutions, improves both J_{sc} and V_{oc} parameters, thus leading to better device efficiencies, so we prepared sensitizing solutions of our dyes, incorporating Cheno as co-adsorbent. Unfortunately, only scarce sensitization occurred in all cases, obtaining, after dipping, soft-colored photoanodes unable to be efficiently photoexcited. In this case, an unbalanced competency between dye and Cheno molecules seems to occur, hampering the anchorage of sensitizing units onto TiO₂ surface.

Figure 5 shows J/V curves for devices sensitized with H₂P and ZnP derivatives, and Table 3 resumes the photovoltaic parameters, short-circuit current (J_{sc}), open circuit voltage (V_{oc}) and fill factor (FF), reflecting much better efficiencies for the zinc compounds. The reason for this difference must be found in the Zn⁺² porphyrin metallic core, a closed shell ion with empty coordination sites, which allow an efficient and rapid injection of photoexcited porphyrin electrons to TiO₂ conduction band, acting as mediator for electron transfer from I⁻/I₃⁻ to the a_{2u} orbital of the porphyrinsensitizer. It is worth to note that the obtained efficiency for device sensitized with ZnP-CO₂H 4 is up to 1.62%, with J_{sc} value of 4.34 mA/cm², V_{oc} of 0.57 V and FF of 0.65, better than that previously reported for the same compound, (1.06%) [33], demonstrating the convenience of our device preparation protocol. On the other hand, ZnP derivatives with two (cis-ZnP-(CO₂H)₂ 5-c) and three (ZnP-(CO₂H)₃ 6) carboxylic acid anchoring groups showed lower results, due a combination of both electronic and structural features. It is well known that efficient dyes usually present the so called push-pull effect, thus facilitating the injection to the TiO₂ conduction band [34]. ZnP-CO₂H 4 shows strong push pull directionality, thanks to the already mentioned electron-acceptor character of the anchoring group and the presence of three electron-donor trimethoxyphenyl substituents in the meso positions. A lesser push pull effect can be found in cis-ZnP-(CO₂H)₂ 5-c and ZnP-(CO₂H)₃ 6. On the other hand, more than one anchoring group means a better anchorage to TiO₂, but not necessarily means better performance. Anchored dyes in

such way could adopt a flat binding position (“face-to-face”, Figure 6a) referred to the TiO₂ surface, offering a lower coverage degree than it does in a perpendicular/vertical fashion (“edge-to-face”, Figure 6b) [35,36]. This is what probably happens, looking to the photovoltaic parameters extracted from J/V curves. The J_{sc} value for ZnP-CO₂H 4 sensitized devices, compared to those sensitized with cis-ZnP-(CO₂H)₂ 5-c and ZnP-(CO₂H)₃ 6 (Table 3), indicates a higher photogenerated current, due to a more compact coverage of the semiconductor surface by the dye. In this context, high values of V_{oc} in ZnP-CO₂H 4 sensitized devices (Table 3), also confirm this hypothesis. High V_{oc} values are indicative of non-aggregated molecules and, in this case, also protection of the central metal core. If ZnP-CO₂H 4 molecules are covering the TiO₂ surface in an “edge-to-face” manner, π-π stacking phenomena seems unlikely to happen between adjacent molecules, due to the necessary non-coplanar position (related to the porphyrin flat structure) of bulky meso-trimethoxyphenyl groups. This results in an effective protection of the porphyrin central metal core, avoiding early recombination processes with the electrolyte, thus affording better V_{oc} values. Same reasoning could be applied to devices sensitized with H₂P derivatives 1–3 but, in this case, the lack of metal ion in the dye becomes crucial. In absence of such mediator, the injection step is slowed down, and early recombination processes are then favored. Interestingly, and opposite to what happens with ZnP 4–6 sensitized devices, structural features of free-base dyes seem to gain weight *vs* electronic characteristics (more than one binding group *vs* push-pull effect). cis-H₂P-(CO₂H)₂ 2-c and H₂P-(CO₂H)₃ 3 sensitized devices show better J_{sc} values than those of H₂P-(CO₂H) 1 (Table 3). This fact indicates that the chromophore is closer to the semiconductor surface, balancing out the absence of metal ion. Furthermore, the number of sterically demanding trimethoxyphenyl groups of the dye, is also reflected in V_{oc} values, higher in the case of cis-H₂P-(CO₂H)₂ 2-c sensitized devices. The presence of two bulky trimethoxyphenyl groups at the meso positions, and only one in the case of H₂P-(CO₂H)₃ 3, partially avoids π-π stacking phenomena between adjacent adsorbed molecules.

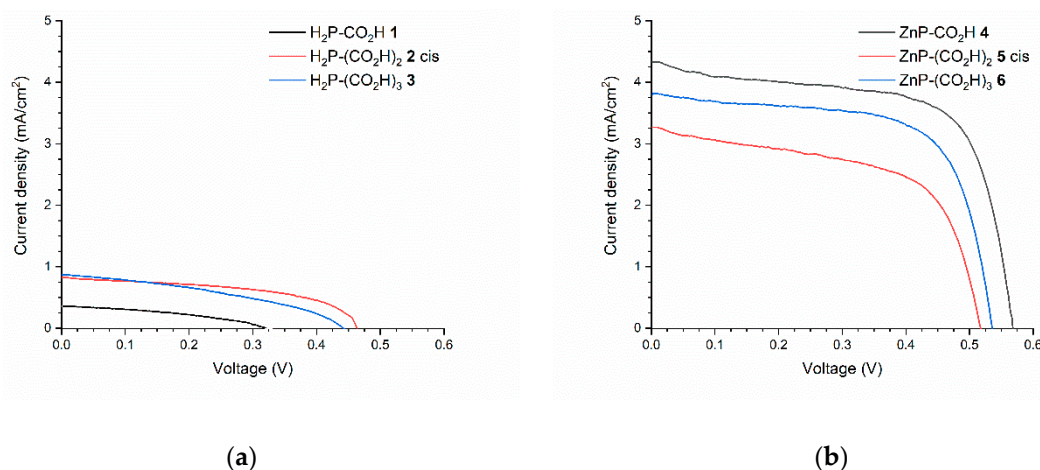


Figure 5. Current density-Voltage curves measured for dye sensitized solar cell (DSSC) devices sensitized with (a) metal-free porphyrins 1–3 and (b) zinc complexes 4–6.

Table 3. Photovoltaic parameters of DSSC devices sensitized with dyes 1–6.

Dye	J _{sc} (mA/cm ²)	V _{oc} (V)	FF	Efficiency (%)
H ₂ P-CO ₂ H 1	0.36	0.32	0.32	0.04
cis-H ₂ P-(CO ₂ H) ₂ 2-c	0.82	0.46	0.52	0.20
H ₂ P-(CO ₂ H) ₃ 3	0.87	0.44	0.38	0.15
ZnP-CO ₂ H 4	4.34	0.57	0.65	1.62
cis-ZnP-(CO ₂ H) ₂ 5-c	3.27	0.52	0.59	0.99
ZnP-(CO ₂ H) ₃ 6	3.79	0.54	0.67	1.36

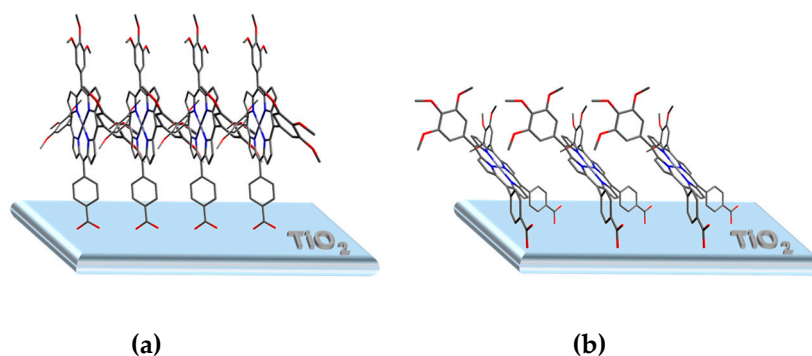


Figure 6. Schematic possible binding geometries of dyes onto TiO_2 surface, (a) “edge-to-face”, and (b) “face-to-face”.

Finally, IPCE measurements were made for all devices, showing maxima of photogenerated current in wavelengths which match the absorption profile of employed sensitizers (Figure 7). As expected, higher performances were obtained for ZnP derivatives 4–6, with maxima at 420, 560 and 600 nm and percentages of 50%, 14%, and 9% respectively in the case of ZnP-CO₂H 4. These results confirm the convenience of introducing just one anchoring place in carboxy ZnP-based sensitizers for DSSCs.

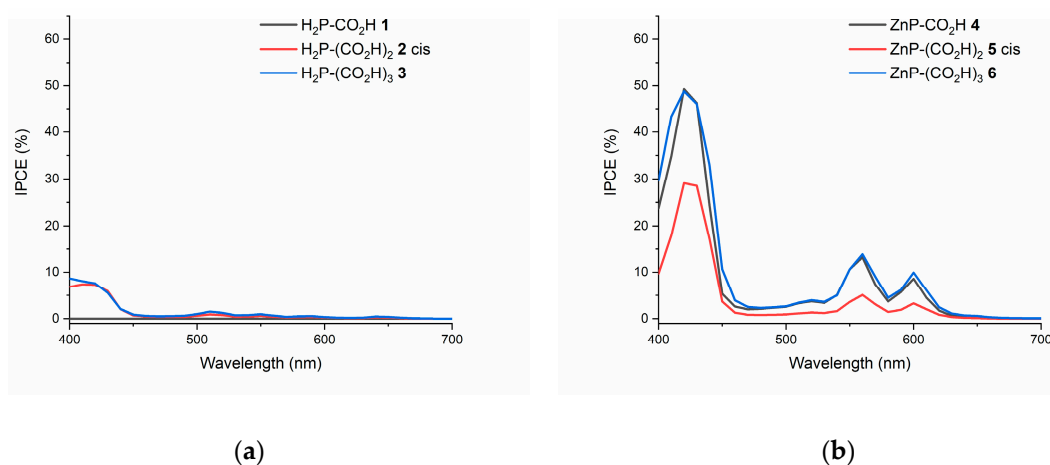


Figure 7. Incident photon-to-current conversion efficiency (IPCE) spectra of DSSC devices sensitized with dyes 1–6.

4. Conclusions

A series of unsymmetric porphyrin compounds, free-base [$\text{H}_2\text{P}-(\text{CO}_2\text{H})_n$ 1–3] and Zn metallated [$\text{ZnP}-(\text{CO}_2\text{H})_n$ 4–6], with one, two or three carboxyphenyl anchoring groups, were synthesized, characterized and used as sensitizers in TiO_2 -based DSSC devices. The comparison of their performances shows the utility of these compounds for this use, reflecting that $\text{ZnP}-(\text{CO}_2\text{H})_n$ 4–6 sensitized solar cells offer better efficiencies, compared to those sensitized with $\text{H}_2\text{P}-(\text{CO}_2\text{H})_n$ 1–3. This is due to the presence of a zinc ion in the porphyrin inner cavity, acting as electronic mediator in the injection step. The observed order of efficiency for the zinc complexes, i.e. $\text{ZnP}-\text{CO}_2\text{H}$ 4 > $\text{ZnP}-(\text{CO}_2\text{H})_3$ 6 > cis- $\text{ZnP}-(\text{CO}_2\text{H})_2$, 5-c is in agreement with a rapid injection of the photoexcited electrons to the TiO_2 conduction band, where electronic characteristics of the dye prevail over its structural features. On the other hand, the observed order of efficiency for free-base dyes, i.e., cis- $\text{H}_2\text{P}-(\text{CO}_2\text{H})_2$ 2-c > ($\text{H}_2\text{P}-(\text{CO}_2\text{H})_3$ 3 > $\text{H}_2\text{P}-\text{CO}_2\text{H}$ 1, agrees with the absence of a metallic mediator, slowing down the injection step and making structural features of the dye to gain prominence over its electronic characteristics.

Supplementary Materials: The following are available online at <http://www.mdpi.com/1996-1944/12/4/650/s1>, Figure S1: Molecular structure of H₂P-CO₂H **1**, Figure S2: ¹H-NMR (CDCl₃) of H₂P-CO₂H **1**, Figure S3: HR-MS (MALDI-TOF) spectrum of H₂P-CO₂H **1**, Figure S4: Molecular structure of cis-H₂P-(CO₂H)₂ **2-c**, Figure S5: ¹H-NMR (CDCl₃) of cis-H₂P-(CO₂H)₂ **2-c**, Figure S6: HR-MS (MALDI-TOF) spectrum of cis-H₂P-(CO₂H)₂ **2-c**, Figure S7: Molecular structure of trans-H₂P-(CO₂H)₂ **2-t**, Figure S8: ¹H-NMR (CDCl₃) of trans-H₂P-(CO₂H)₂ **2-t**, Figure S9: HR-MS (MALDI-TOF) spectrum of trans-H₂P-(CO₂H)₂ **2-t**, Figure S10: Molecular structure of H₂P-(CO₂H)₃ **3**, Figure S11: ¹H-NMR (CDCl₃) of H₂P-(CO₂H)₃ **3**, Figure S12: HR-MS (MALDI-TOF) spectrum of H₂P-(CO₂H)₃ **3**, Figure S13: Molecular structure of ZnP-CO₂H **4**, Figure S14: ¹H-NMR (CDCl₃) of ZnP-CO₂H **4**, Figure S15: HR-MS (MALDI-TOF) spectrum of ZnP-CO₂H **4**, Figure S16: Molecular structure of cis-ZnP-(CO₂H)₂ **5-c**, Figure S17: ¹H-NMR (CDCl₃) of cis-ZnP-(CO₂H)₂ **5-c**, Figure S18: HR-MS (MALDI-TOF) spectrum of cis-ZnP-(CO₂H)₂ **5-c**, Figure S19: Molecular structure of trans-ZnP-(CO₂H)₂ **5-t**, Figure S20: ¹H-NMR (CDCl₃) of trans-ZnP-(CO₂H)₂ **5-t**, Figure S21: HR-MS (MALDI-TOF) spectrum of trans-ZnP-(CO₂H)₂ **5-t**, Figure S22: Molecular structure of ZnP-(CO₂H)₃ **6**, Figure S23: ¹H-NMR (CDCl₃) of ZnP-(CO₂H)₃ **6**, Figure S24: HR-MS (MALDI-TOF) spectrum of ZnP-(CO₂H)₃ **6**, Figure S25: Molecular structure of H₂P-CO₂Me **7**, Figure S26: ¹H-NMR (CDCl₃) of H₂P-CO₂Me **7**, Figure S27: HR-MS (MALDI-TOF) spectrum of H₂P-CO₂Me **7**, Figure S28: Molecular structure of H₂P-(CO₂Me)₂ **8** mixture of isomers, Figure S29: ¹H-NMR (CDCl₃) of H₂P-(CO₂Me)₂ **8** mixture of isomers, Figure S30: HR-MS (MALDI-TOF) spectrum of H₂P-(CO₂Me)₂ **8** mixture of isomers, Figure S31: Molecular structure of H₂P-(CO₂Me)₃ **9**, Figure S32: ¹H-NMR (CDCl₃) of H₂P-(CO₂Me)₃ **9**, Figure S33: HR-MS (MALDI-TOF) spectrum of H₂P-(CO₂Me)₃ **9**.

Author Contributions: A.S.-S. directed the research. The project was initially proposed by S.Z., R.N. performed the experimental work and characterized all compounds, materials and devices. R.N., L.M.-G., F.F.-L., S.Z., and A.S.-S. wrote the manuscript.

Funding: Support from the Ministerio de Economía Industria y Competitividad of Spain (CTQ2017-87102-R) is gratefully acknowledged.

Conflicts of Interest: The authors declare no conflict of interest.

References

- Kundu, S.; Patra, A. Nanoscale Strategies for Light Harvesting. *Chem. Rev.* **2017**, *117*, 712–757. [[CrossRef](#)]
- Zhang, J.; Wang, J.; Long, S.; Peh, S.B.; Dong, J.; Wang, Y.; Karmakar, A.; Yuan, Y.D.; Cheng, Y.; Zhao, D. Luminescent Metal–Organic Frameworks for the Detection and Discrimination of o-Xylene from Xylene Isomers. *Inorg. Chem.* **2018**, *57*, 13631–13639. [[CrossRef](#)]
- Acherar, S.; Colombeau, L.; Frochot, C.; Vanderesse, R. Synthesis of Porphyrin, Chlorin and Phthalocyanine Derivatives by Azide-Alkyne Click Chemistry. *Curr. Med. Chem.* **2015**, *22*, 3217–3254. [[CrossRef](#)] [[PubMed](#)]
- Stulz, E. Nanoarchitectonics with Porphyrin Functionalized DNA. *Acc. Chem. Res.* **2017**, *50*, 823–831. [[CrossRef](#)] [[PubMed](#)]
- Mahmood, A.; Hu, J.-Y.; Xiao, B.; Tang, A.; Wang, X.; Zhou, E. Recent progress in porphyrin-based materials for organic solar cells. *J. Mater. Chem. A* **2018**, *6*, 16769–16797. [[CrossRef](#)]
- Song, H.; Liu, Q.; Xie, Y. Porphyrin-sensitized solar cells: Systematic molecular optimization, coadsorption and cosensitization. *Chem. Commun.* **2018**, *54*, 1811–1824. [[CrossRef](#)] [[PubMed](#)]
- Di Carlo, G.; Biroli, A.O.; Tessore, F.; Caramori, S.; Pizzotti, M. β -Substituted Zn II porphyrins as dyes for DSSC: A possible approach to photovoltaic windows. *Coord. Chem. Rev.* **2018**, *358*, 153–177. [[CrossRef](#)]
- Birel, Ö.; Nadeem, S.; Duman, H. Porphyrin-Based Dye-Sensitized Solar Cells (DSSCs): A Review. *J. Fluoresc.* **2017**, *27*, 1075–1085. [[CrossRef](#)] [[PubMed](#)]
- Ladomenou, K.; Kitsopoulos, T.N.; Sharma, G.D.; Coutsolelos, A.G. The importance of various anchoring groups attached on porphyrins as potential dyes for DSSC applications. *RSC Adv.* **2014**, *4*, 21379–21404. [[CrossRef](#)]
- Santos, T.D.; Morandeira, A.; Koops, S.; Mozer, A.J.; Tsekouras, G.; Dong, Y.; Wagner, P.; Wallace, G.; Earles, J.C.; Gordon, K.C.; et al. Injection Limitations in a Series of Porphyrin Dye-Sensitized Solar Cells. *J. Phys. Chem. C* **2010**, *114*, 3276–3279. [[CrossRef](#)]
- Higashino, T.; Sugiura, K.; Tsuji, Y.; Nimura, S.; Ito, S.; Imahori, H. A Push–Pull Porphyrin Dimer with Multiple Electron-donating Groups for Dye-sensitized Solar Cells: Excellent Light-harvesting in Near-infrared Region. *Chem. Lett.* **2016**, *45*, 1126–1128. [[CrossRef](#)]
- Chaudhri, N.; Sawhney, N.; Madhusudhan, B.; Raghav, A.; Sankar, M.; Satapathi, S. Effect of functional groups on sensitization of dye-sensitized solar cells (DSSCs) using free base porphyrins. *J. Porphyr. Phthalocyanines* **2017**, *21*, 222–230. [[CrossRef](#)]

13. Xiang, H.; Fan, W.; Li, J.H.; Li, T.; Robertson, N.; Song, X.; Wu, W.; Wang, Z.; Zhu, W.; Tian, H. High Performance Porphyrin-Based Dye-Sensitized Solar Cells with Iodine and Cobalt Redox Shuttles. *ChemSusChem* **2017**, *10*, 938–945. [[CrossRef](#)] [[PubMed](#)]
14. Parsa, Z.; Naghavi, S.S.; Safari, N. Designing Push–Pull Porphyrins for Efficient Dye-Sensitized Solar Cells. *J. Phys. Chem. A* **2018**, *122*, 5870–5877. [[CrossRef](#)] [[PubMed](#)]
15. Martínez-Díaz, M.V.; de la Torre, G.; Torres, T. Lighting porphyrins and phthalocyanines for molecular photovoltaics. *Chem. Commun.* **2010**, *46*, 7090. [[CrossRef](#)] [[PubMed](#)]
16. Reddy, K.S.K.; Liu, Y.-C.; Chou, H.-H.; Kala, K.; Wei, T.-C.; Yeh, C.-Y. Synthesis and Characterization of Novel β -Bis(N,N-diaryl-amino)-Substituted Porphyrin for Dye-Sensitized Solar Cells under 1 sun and Dim Light Conditions. *ACS Appl. Mater. Interfaces* **2018**, *10*, 39970–39982. [[CrossRef](#)]
17. Wu, S.-L.; Lu, H.-P.; Yu, H.-T.; Chuang, S.-H.; Chiu, C.-L.; Lee, C.-W.; Diao, E.W.-G.; Yeh, C.-Y. Design and characterization of porphyrin sensitizers with a push-pull framework for highly efficient dye-sensitized solar cells. *Energy Environ. Sci.* **2010**, *3*, 949–955. [[CrossRef](#)]
18. Imahori, H.; Matsubara, Y.; Iijima, H.; Umeyama, T.; Matano, Y.; Ito, S.; Niemi, M.; Tkachenko, N.V.; Lemmetyinen, H. Effects of meso-Diaryl-amino Group of Porphyrins as Sensitizers in Dye-Sensitized Solar Cells on Optical, Electrochemical, and Photovoltaic Properties. *J. Phys. Chem. C* **2010**, *114*, 10656–10665. [[CrossRef](#)]
19. Sirithip, K.; Prachumrak, N.; Rattanawan, R.; Keawin, T.; Sudyoadsuk, T.; Namuangruk, S.; Jungstittiwong, S.; Promarak, V. Zinc–Porphyrin Dyes with Different meso-Aryl Substituents for Dye-Sensitized Solar Cells: Experimental and Theoretical Studies. *Chem. Asian J.* **2015**, *10*, 882–893. [[CrossRef](#)]
20. Keawin, T.; Tarsang, R.; Sirithip, K.; Prachumrak, N.; Sudyoadsuk, T.; Namuangruk, S.; Roncali, J.; Kungwan, N.; Promarak, V.; Jungstittiwong, S. Anchoring number-performance relationship of zinc-porphyrin sensitizers for dye-sensitized solar cells: A combined experimental and theoretical study. *Dyes Pigm.* **2017**, *136*, 697–706. [[CrossRef](#)]
21. Rangan, S.; Coh, S.; Bartynski, R.A.; Chitre, K.P.; Galoppini, E.; Jaye, C.; Fischer, D. Energy Alignment, Molecular Packing, and Electronic Pathways: Zinc(II) Tetraphenylporphyrin Derivatives Adsorbed on TiO₂(110) and ZnO(11–20) Surfaces. *J. Phys. Chem. C* **2012**, *116*, 23921–23930. [[CrossRef](#)]
22. Urbani, M.; Grätzel, M.; Nazeeruddin, M.K.; Torres, T. Meso-Substituted Porphyrins for Dye-Sensitized Solar Cells. *Chem. Rev.* **2014**, *114*, 12330–12396. [[CrossRef](#)]
23. Ambre, R.B.; Mane, S.B.; Chang, G.-F.; Hung, C.-H. Effects of Number and Position of Meta and Para Carboxyphenyl Groups of Zinc Porphyrins in Dye-Sensitized Solar Cells: Structure–Performance Relationship. *ACS Appl. Mater. Interfaces* **2015**, *7*, 1879–1891. [[CrossRef](#)]
24. Adler, A.D.; Longo, F.R.; Finarelli, J.D.; Goldmacher, J.; Assour, J.; Korsakoff, L. A simplified synthesis for meso-tetraphenylporphyrine. *J. Org. Chem.* **1967**, *32*, 476. [[CrossRef](#)]
25. Gouterman, M. Spectra of Porphyrins. *J. Mol. Spectrosc.* **1961**, *6*, 138–163. [[CrossRef](#)]
26. Gierschner, J.; Cornil, J.; Egelhaaf, H.-J. Optical Bandgaps of π -Conjugated Organic Materials at the Polymer Limit: Experiment and Theory. *Adv. Mater.* **2007**, *19*, 173–191. [[CrossRef](#)]
27. Shi, W.; Peng, B.; Guo, Y.; Lin, L.; Peng, T.; Li, R. Synthesis of asymmetric zinc phthalocyanine with bulky diphenylthiophenol substituents and its photovoltaic performance for dye-sensitized solar cells. *J. Photochem. Photobiol. A Chem.* **2016**, *321*, 248–256. [[CrossRef](#)]
28. Zhou, Y.; He, Q.; Yang, Y.; Zhong, H.; He, C.; Sang, G.; Liu, W.; Yang, C.; Bai, F.; Li, Y. Binaphthyl-Containing Green- and Red-Emitting Molecules for Solution-Processable Organic Light-Emitting Diodes. *Adv. Funct. Mater.* **2008**, *18*, 3299–3306. [[CrossRef](#)]
29. Meot-Ner, M.; Adler, A.D. Substituent effects in noncoplanar pi systems: meso-Porphyrins. *J. Am. Chem. Soc.* **1975**, *97*, 5107–5111. [[CrossRef](#)]
30. Grätzel, M. Photoelectrochemical cells. *Nature* **2001**, *414*, 338–344. [[CrossRef](#)]
31. Eu, S.; Katoh, T.; Umeyama, T.; Matano, Y.; Imahori, H. Synthesis of sterically hindered phthalocyanines and their applications to dye-sensitized solar cells. *Dalton Trans.* **2008**, 5476–5483. [[CrossRef](#)] [[PubMed](#)]
32. Pavlishchuk, V.V.; Addison, A.W. Conversion constants for redox potentials measured versus different reference electrodes in acetonitrile solutions at 25 °C. *Inorg. Chim. Acta* **2000**, *298*, 97–102. [[CrossRef](#)]
33. Tan, Q.; Zhang, X.; Mao, L.; Xin, G.; Zhang, S. Novel zinc porphyrin sensitizers for dye-sensitized solar cells: Synthesis and spectral, electrochemical, and photovoltaic properties. *J. Mol. Struct.* **2013**, *1035*, 400–406. [[CrossRef](#)]

34. Martin-Gomis, L.; Fernández-Lázaro, F.; Sastre-Santos, Á. Advances in phthalocyanine-sensitized solar cells (PcSSCs). *J. Mater. Chem. A* **2014**, *2*, 15672–15682. [[CrossRef](#)]
35. Cherian, S.; Wamser, C.C. Adsorption and Photoactivity of Tetra(4-carboxyphenyl)porphyrin (TCPP) on Nanoparticulate TiO₂. *J. Phys. Chem. B* **2000**, *104*, 3624–3629. [[CrossRef](#)]
36. Rochford, J.; Chu, D.; Hagfeldt, A.; Galoppini, E. Tetrachelate Porphyrin Chromophores for Metal Oxide Semiconductor Sensitization: Effect of the Spacer Length and Anchoring Group Position. *J. Am. Chem. Soc.* **2007**, *129*, 4655–4665. [[CrossRef](#)]



© 2019 by the authors. Licensee MDPI, Basel, Switzerland. This article is an open access article distributed under the terms and conditions of the Creative Commons Attribution (CC BY) license (<http://creativecommons.org/licenses/by/4.0/>).